Published online 23 March 2018 *Nucleic Acids Research, 2018, Vol. 46, No. 8* ***4271–4285***
doi: 10.1093/nar/gky223

Loss of RNA-binding protein HuR facilitates cellular senescence through posttranscriptional regulation of *TIN2* mRNA

Ji Hoon Lee[1], Misun Jung[2], Juyeong Hong[1], Mi Kyung Kim[1] and In Kwon Chung[1,2,*]

[1]Department of Systems Biology, College of Life Science and Biotechnology, Yonsei University, Seoul 03722, Korea and [2]Department of Integrated Omics for Biomedical Science, Yonsei University, Seoul 03722, Korea

Received July 21, 2017; Revised March 10, 2018; Editorial Decision March 14, 2018; Accepted March 15, 2018

ABSTRACT

Cellular senescence can be induced by high levels of reactive oxygen species (ROS) produced by mitochondria. However, the mechanism by which elevated mitochondrial ROS levels are produced during replicative senescence is not yet fully understood. Here, we report that loss of the RNA-binding protein, human antigen R (HuR), during replicative senescence leads to an increase in ROS levels through enhanced mitochondrial localization of the telomeric protein TIN2. HuR binds to the 3′ untranslated region of *TIN2* mRNA. This association decreases TIN2 protein levels by both destabilizing *TIN2* mRNA and reducing its translation. Conversely, depletion of HuR levels enhances TIN2 expression, leading to increased mitochondrial targeting of TIN2. Mitochondrial localization of TIN2 increases ROS levels, which contributes to induction and maintenance of cellular senescence. Our findings provide compelling evidence for a novel role of HuR in controlling the process of cellular senescence by regulating TIN2-mediated mitochondrial ROS production, and for a useful therapeutic route for modulating intracellular ROS levels in treating both aging-related complications and cancer.

INTRODUCTION

Telomeres are specialized nucleoprotein complexes that are essential for the stability and protection of chromosome ends and have been implicated in aging and cancer development (1,2). Mammalian telomeres consist of long tracts of duplex TTAGGG repeats with 3′ single-stranded G overhangs and are tightly associated with numerous copies of six-protein complexes called shelterin (3,4). Three shelterin proteins, TRF1, TRF2, and POT1, directly recognize telomeric repeats and are associated with three additional proteins, TIN2, TPP1 and RAP1. The shelterin complex protects the natural chromosome ends from being incorrectly identified as double-strand DNA breaks (5,6). Although the shelterin complex functions as a unit, individual components have distinct roles in the regulation of telomere function. Functional alteration of the shelterin proteins can lead to telomere loss, inappropriate DNA repair reactions, and DNA damage response at telomeres.

TIN2 plays a central role in the assembly and structural integrity of shelterin complexes through its ability to interact with TRF1, TRF2 and TPP1 (7,8). TIN2 binding to TPP1 connects the TPP1/POT1 heterodimer to TRF1 and TRF2 on duplex telomeric repeats, allowing POT1 to associate with single-stranded telomeric DNA (9–11). Depletion of TIN2 removes the telomere's protection by destabilizing the shelterin complex, causing activation of telomeric DNA damage signaling (12,13). TPP1 regulates telomerase recruitment to telomeres through the interaction of its N-terminal OB-fold domain with telomerase reverse transcriptase (TERT). This interaction is crucial for maintenance of telomere length (14–16). Due to its ability to interact with TPP1, functional inhibition of TIN2 results in reduced levels of TPP1-mediated telomerase recruitment to telomeres, suggesting an indirect role for TIN2 in the regulation of telomere length homeostasis (17,18). In humans, loss-of-function mutations in TIN2 have been associated with a number of diseases including dyskeratosis congenita, aplastic anemia, pulmonary fibrosis, and multiple types of cancer (19–22).

In addition to its role in telomere maintenance, TIN2 can also localize to the mitochondria, where it is post-translationally processed and can regulate oxidative phosphorylation (23,24). The N-terminal region of TIN2 is essential for targeting TIN2 to the mitochondria, and also for interaction with TPP1 (25). Whereas truncation of the 18 N-terminal amino acids in TIN2 disrupts TPP1 binding and enhances mitochondrial localization, mutations that disrupt the mitochondrial localization sequence maintain TPP1 binding and facilitate TPP1's nuclear localization. In addition, depletion of TIN2 increases mitochondrial ATP production and oxygen consumption, and inhibits ROS

*To whom correspondence should be addressed. Tel: +822 2123 2660; Fax: +822 364 8660; Email: topoviro@yonsei.ac.kr

generation (23). These findings suggest that TIN2 likely participate in the regulation of mitochondrial function independent of its role in telomere maintenance (23,24).

HuR is a ubiquitously expressed member of the Hu RNA-binding protein family and has been implicated in various biological processes (26–30). Through its binding to AU-rich elements (AREs), which are typically located in 3′ untranslated regions (3′UTRs), HuR regulates the stability, translation, and subcellular distribution of target mRNAs. In many cases, HuR has been shown to stabilize various target mRNAs (31–36). However, some studies have revealed that HuR regulates target mRNA expression by reducing mRNA stability (37,38). Thus, the biological consequence of HuR association with mRNAs varies depending on the precise target mRNA involved. Interestingly, HuR levels are markedly reduced in human fibroblasts undergoing replicative senescence and in aged human tissues (39–42). Indeed, depletion of HuR accelerates the senescent phenotype, while overexpression of HuR delays replicative senescence. Therefore, it is widely assumed that HuR is involved in replicative senescence by regulating the expression of multiple senescence-related genes.

Although ROS produced by mitochondria indisputably plays an important role in senescence (43–45), important questions include how elevated mitochondrial ROS levels are produced during replicative senescence. In this work, we examined whether HuR regulates the expression of telomere binding proteins. We found that HuR decreases TIN2 protein levels by both destabilizing *TIN2* mRNA and reducing its translation. We also show that depletion of HuR levels enhances TIN2 expression and increases mitochondrial targeting of TIN2 in both primary human fibroblasts and human cancer cells. In our model, mitochondrial localization of TIN2 leads to an increase in ROS levels, which in turn triggers or accelerates cellular senescence. These results suggest that HuR controls some aspects of cellular senescence by regulating TIN2-mediated mitochondrial ROS levels.

MATERIALS AND METHODS

Cell culture and plasmids

Human cervical carcinoma HeLa cells and human fetal lung fibroblast IMR-90 were cultured in Dulbecco's modified Eagle's medium, and human osteosarcoma U2OS cells were cultured in McCoy's modified medium supplemented with 10% fetal bovine serum, 100 units/mL penicillin, and 100 μg/mL streptomycin in 5% CO_2 at 37°C. The expression vectors for Flag-HuR and TIN2-Myc were constructed by inserting the respective full-length cDNAs into pLNCX2 (Clontech) and pcDNA6/myc-His A (Invitrogen), respectively. The TIN2-F37D/L38E, TIN2-L48E and TIN2-K62A/K64A plasmids were generated by site-directed mutagenesis using the QuikChange II kit according to the manufacturer's instructions (Stratagene). GFP-TIN2 3′UTR plasmids were constructed by inserting the full-length and truncated 3′UTR fragments into pEGFP-C1 plasmid (Clontech) as indicated. All constructs were verified by DNA sequencing.

Establishment of stable cell lines

The retrovirus vectors were constructed by cloning the shRNA oligonucleotides for targeting HuR (5′-GATCC CCGTCTGTTCAGCAGCATTGGTTCAAGAGACC AATGCTGCTGAACAG ACTTTTTA-3′ for shHuR-1; 5′-GATCCCCTGTGAAAGTGATTCGTGATTTCAA GAGAATC ACGAATCACTTTCACATTTTTA-3′ for shHuR-2) into a pSUPER.retro.puro vector (Oligoengine) and transfected into HEK293T packaging cells with pGP (for *gag-pol* expression) and pE-ampho (for *env* expression) vectors according to the manufacturer's instructions (TAKARA). After 48 h, the culture supernatants were harvested and filtered through a 0.45 μm filter. HeLa cells were transduced with the viral supernatants containing 4 μg/ml polybrene (Sigma-Aldrich). After selection with 1 μg/ml puromycin (Gibco), stable cell lines were established as mass cultures from separate transductions and checked for protein expression by immunoblot analysis with anti-HuR antibodies.

Quantitative RT-PCR analysis

Total RNA was extracted from HeLa cells using Easy-BLUE (Intron). The reverse transcription reaction was performed with 1 μg of total RNA using random primer and M-MLV reverse transcriptase (Promega). cDNA was used for quantitative PCR. For isolation of mRNA bound to HuR, immunoprecipitation was performed using a HuR-specific antibody. The immunoprecipitation materials were incubated with proteinase K at 45°C for 1 h and then used for reverse transcription. For quantitative real-time PCR, each PCR reaction contained cDNA, gene-specific primer pairs, and TOPreal™ qPCR 2X PreMIX (SYBR Green with high ROX) according to the manufacturer's instructions (Enzynomics). GAPDH primers were used as an endogenous reference. Primer pairs are listed in Supplementary Table S1. Reactions were performed in triplicate for each sample and were analyzed using the ABI PRISM 7300 Sequence Detection System (Applied Biosystems). Quantitative RT-PCRs were carried out following the MIQE guidelines, and an MIQE checklist is provided in Supplementary Table S2 (46).

Immunoblotting and immunoprecipitation

Immunoblotting and IP were performed as previously described (47). The expression vectors were transiently transfected using Lipofectamine 3000 reagent according to the manufacturer's protocol (Invitrogen). Cells were resuspended in lysis buffer (0.5% NP-40, 1.5 mM $MgCl_2$, 25 mM HEPES–KOH, pH 7.5, 150 mM KCl, 10% glycerol, and proteinase inhibitor cocktail), and incubated on ice for 30 min. Lysates were clarified by centrifugation at 16 000 × *g* for 15 min at 4°C to remove insoluble material. For IP, the supernatants were pre-cleared with either mouse or rabbit IgG (Santa Cruz Biotechnology) and protein A sepharose beads (GE Healthcare) for 30 min at 4°C and then incubated with primary antibodies at 4°C overnight, followed by incubation with protein A-Sepharose beads for 1 h. After binding, the beads were washed extensively with lysis buffer and subjected to immunoblot analysis.

IP and immunoblotting were performed using anti-Flag (M2, Sigma), HuR (3A2, Santa Cruz Biotechnology), GFP (B-2, Santa Cruz Biotechnology), dyskerin (H-300, Santa Cruz Biotechnology), TRF1 (C-19, Santa Cruz Biotechnology), TRF2 (D1Y5D, Cell Signaling Technology), RAP1 (A300-306A, Bethyl Laboratories), POT1 (ab21382, Abcam), TPP1 (ab54685, Abcam), TIN2 (ab136997, Abcam), Lamin A/C (N-18, Santa Cruz Biotechnology), p53 (FL-393, Santa Cruz Biotechnology), p21 (C-19, Santa Cruz Biotechnology), p16 (H-43, Santa Cruz Biotechnology), and tubulin (TU-02, Santa Cruz Biotechnology), as specified. All immunoblots are representative of at least three experiments that demonstrated similar results.

Polysome analysis

Cells were transfected with empty vector or Flag-HuR and incubated with 100 μg/ml cycloheximide for 10 min and lysed with polysome extraction buffer containing 20 mM Tris–HCl, pH 7.5, 100 mM KCl, 5 mM $MgCl_2$ and 0.5% NP-40 as previously described (48). Cytoplasmic lysates were fractionated by ultracentrifugation through 10–50% linear sucrose gradients and divided into 24 fractions. The total RNA in each fraction was extracted with Easy-BLUE (Intron) and analyzed by quantitative RT-PCR analysis.

Immunofluorescence and telomere fluorescence *in situ* hybridization (FISH)

Immunofluorescence and FISH were performed by modifying existing protocols (49). Briefly, cells grown on glass coverslips were fixed with 4% paraformadehyde in PBS for 10 min, permeabilized in PBS containing 0.5% Triton X-100 for 10 min, and then blocked with PBS containing 0.5% bovine serum albumin and 0.2% cold fish gelatin for 10 min. Cells were then incubated with mouse anti-TIN2, mouse anti-Myc, and rabbit anti-TOM20 for 16 h at 4°C. After thorough washing with PBS, cells were incubated with Alexa Fluor 488-conjugated anti-rabbit immunoglobulin and Alexa Fluor 568-conjugated anti-mouse immunoglobulin (Molecular Probes). For TIF analysis, cells were incubated with rabbit anti-53BP1 (sc-22760, Santa Cruz Biotechnology) or rabbit anti-γH2AX (2577, Cell Signaling Technology), followed by incubation with Alexa Fluor 488-conjugated anti-rabbit immunoglobulin. Telomere FISH staining was performed with Cy3-$(CCCTAA)_3$ peptide nucleic acid probe (Panagene) as previously described (50). Cells were counterstained with 4,6-diamino-2-phenylindole (DAPI) (Vectashield; Vector Laboratories). Immunofluorescence images were captured using a confocal laser-scanning microscope LSM 700 (Carl Zeiss).

Detection of mitochondrial superoxide production

Mitochondrial superoxide levels were measured with a MitoSOX™ Red mitochondrial superoxide indicator according to the manufacturer's instructions (Invitrogen). The fluorescent signals were collected in the FL2-H channel of a FACSCalibur flow cytometry and analyzed using CellQuest software (BD Bioscience). Results were analyzed by the 'M2 percentage' fluorescence variation using Flowing Software 2.0. M2 indicates the percentage of cells with enhanced ROS production. To determine the absolute superoxide levels in control and HuR knockdown cells, the MitoSOX Red fluorescent signals were corrected in the PE channel of a flow cytometer (Beckman Coulter CytoFLEX). The mean fluorescence levels measured from unstained cells were subtracted from the levels of the MitoSOX Red stained cells. The superoxide levels were presented as the relative mean fluorescent intensity compared to the average level of control.

Imaging of mitochondrial superoxide production

For fluorescence microscopy image, increased fluorescence of MitoSOX Red was used as an assay for mitochondrial superoxide production. Cells were incubated with 5 μM of MitoSOX Red for 10 min and counterstained with 4,6-diamino-2-phenylindole (DAPI) prior to fluorescence measurement using a confocal laser-scanning microscope LSM 700 (Carl Zeiss). The fluorescence intensity was quantified using ImageJ software. The results represent relative fluorescence intensity normalized to controls.

Cell cycle analysis

Cells were washed with PBS and fixed for 30 min in ice-cold 70% ethanol. Cells were resuspended in PBS containing RNase A (200 μg/ml) and propidium iodide (50 μg/ml) and incubated in the dark for 30 min at room temperature. Cell cycle distribution was monitored by flow cytometry using a FACScan flow cytometer (BD Biosciences).

Cellular fractionation

Mitochondrial and cytosolic fractions were obtained using the Mitochondria/Cytosol Fractionation Kit according to the manufacturer's instructions (BioVision). Briefly, cells were resuspended in cytosol isolation buffer mix, homogenized by an ice-cold tissue homogenizer, and centrifuged at 700 × *g* for 10 min at 4°C. The supernatant was recentrifuged at 10 000 × *g* for 30 min in 4°C, and the pelleted mitochondrial fraction was resuspended in mitochondria isolation buffer mix. To obtain the nuclear fraction, cells were resuspended in hypotonic buffer (10 mM HEPES–KOH, pH 7.9, 1.5 mM $MgCl_2$, 10 mM KCl, 0.5 mM DTT, 0.2 mM phenyl methylsulphonyl fluoride) for 10 min on ice, followed by addition of 0.625% NP-40 for 20 min. After centrifugation at 14 000 × *g* for 5 min at 4°C, the nuclear pellets were resuspended in nuclear extraction buffer (20 mM HEPES–KOH, pH 7.9, 25% Glycerol, 420 mM NaCl, 1.5 mM $MgCl_2$, 0.2 mM EDTA, 0.5 mM DTT, 0.2 mM phenyl methylsulphonyl fluoride) for 20 min on ice and centrifuged at 14 000 × *g* for 20 min at 4°C. The supernatant was collected as the nuclear fraction.

Senescence-associated β-galactosidase assay

Senescence-associated β-galactosidase assays were performed as previously described (51). Briefly, cells were plated in side culture chambers and washed with PBS, followed by fixation with 2% formaldehyde/0.2% glutaraldehyde for 5 min. Cells were then incubated for 12 h with

senescence-associated β-galactosidase staining solution (1 mg/ml X-gal, 40 mM citric acid/sodium phosphate, pH 6, 5 mM potassium ferrocyanide, 5 mM ferricyanide, 150 mM NaCl and 2 mM $MgCl_2$).

Statistical analysis

All data are presented as the means ± standard error of the means from three independent experiments. Statistical analyses were performed using a two-tailed, equal-sample variance Student's *t*-test. *P* values <0.05 were considered statistically significant.

RESULTS

HuR represses TIN2 expression levels by both destabilizing *TIN2* mRNA and reducing its translation

Given that HuR controls the stability, translation, and intracellular localization of various target mRNAs (28), we set out to investigate whether HuR regulates the expression of mRNAs encoding shelterin proteins in HeLa cells. Immunoprecipitation (IP) reactions were performed to isolate mRNA bound to endogenous HuR using HuR-specific antibodies. The identification of mRNA from the immunoprecipitated material was achieved by quantitative reverse transcription-polymerase chain reaction (RT-PCR) analysis. Among the six shelterin mRNAs tested, *TIN2* mRNA alone was highly enriched in HuR immunoprecipitated samples compared to IgG controls (Figure 1A). We also examined functional links between HuR and telomerase holoenzyme components and found that HuR did not interact with mRNAs encoding telomerase holoenzyme components (Supplementary Figure S1). In addition, we determined that HuR also interacts only with *TIN2* mRNA in telomerase-negative U2OS cells (Supplementary Figure S2). These results indicate that *TIN2* mRNA could be a target of HuR in both telomerase positive and negative cancer cell lines.

To investigate the role of HuR in the regulation of TIN2 expression, we examined the effect of HuR overexpression on TIN2 levels. The expression of Flag-HuR in HeLa cells reduced the overall levels of TIN2 protein (Figure 1B). This alteration is specific for TIN2 because overexpression of HuR did not influence the levels of other shelterin proteins. Reduction in TIN2 caused by HuR overexpression did not reverse upon treatment with the proteasome inhibitor MG132, indicating that HuR does not influence TIN2 protein stability (Figure 1C). To further verify these findings, HeLa cells transfected with Flag-HuR were incubated with cycloheximide to block new protein synthesis and analyzed by immunoblot to detect TIN2 levels. The half-life of TIN2 was not significantly altered by HuR overexpression compared to empty vector control (Supplementary Figure S3). We also found that none of the shelterin proteins and telomerase components interacted with HuR (Supplementary Figure S4).

To gain insight into how HuR represses TIN2 expression, we assessed the levels of *TIN2* mRNA in cells expressing Flag-HuR by quantitative RT-PCR. Overexpression of HuR decreased the levels of *TIN2* mRNA, but did not affect the levels of other shelterin mRNAs (Figure 1D), implying that HuR overexpression reduces the stability of *TIN2* mRNA. To further confirm these findings, cells were treated with actinomycin D to block *de novo* mRNA synthesis. Total cellular RNA was extracted at the indicated times and subjected to RT-PCR to determine the half-life of *TIN2* mRNA. As shown in Figure 1E, the half-life of *TIN2* mRNA in HuR-expressing cells was significantly shortened compared to empty vector-expressing control cells. Together, these results suggest that HuR interacts with the *TIN2* mRNA and represses TIN2 expression at least in part by destabilizing *TIN2* mRNA.

In addition to regulating target mRNA stability, HuR also modulates the translation of some target mRNAs (52). To test the possibility that HuR may influence TIN2 translation, we performed polysome analysis in cells transfected with Flag-HuR. Cytoplasmic lysates were fractionated through sucrose gradients to separate ribosomal subunits (40S and 60S), monosomes (80S) and progressively larger polysomes (Figure 1F). Overexpression of HuR did not change the overall polysome distribution profiles. RNA was extracted from each of the 24 fractions, and the levels of *TIN2* and *GAPDH* mRNAs were quantified by quantitative RT-PCR analysis. Whereas *TIN2* mRNA levels peaked at fraction 16 in control cells, the distribution of *TIN2* mRNA shifted leftward when HuR was overexpressed, peaking at fraction 11, indicating that *TIN2* mRNA formed on average smaller polysomes after HuR overexpression (Figure 1F). The distribution of *GAPDH* mRNA was not affected by HuR overexpression. Overall, these results suggest that HuR represses TIN2 expression levels by both destabilizing *TIN2* mRNA and reducing its translation.

HuR represses TIN2 expression through the TIN2 3′UTR

To find the region at which HuR binds *TIN2* mRNA, we constructed a GFP-derived reporter plasmid bearing the TIN2 3′UTR (Figure 2A). Overexpression of Flag-HuR reduced the expression of GFP protein from the chimeric plasmid, pGFP-TIN2 3′UTR, but did not affect the control plasmid, pGFP (Figure 2B). The levels of GFP-TIN2 3′UTR transcript were also decreased by HuR overexpression. In contrast, depletion of HuR by short hairpin RNA (shRNA) increased the levels of both GFP protein and mRNA from the pGFP-TIN2 3′UTR, but not from the pGFP (Figure 2C). These results demonstrate that HuR represses TIN2 expression through an interaction with TIN2's 3′UTR.

To determine the HuR binding region within the 3′UTR of *TIN2* mRNA, we divided the TIN2 3′UTR into four fragments and constructed a series of GFP-derived reporter constructs bearing FL (full-length 3′UTR), A, B, C, or D fragments (Figure 2D). HeLa cells were transfected with GFP-derived reporter constructs and subjected to IP with anti-HuR antibodies in order to identify the TIN2 3′UTR region bound to HuR. The results showed that endogenous HuR interacts with full-length 3′UTR and fragment B, but not with fragments A, C or D (Figure 2E). Moreover, overexpression of Flag-HuR reduced the levels of GFP expression in cells expressing pGFP-FL and pGFP-B (Figure 2F). We also performed RT-PCR to assess the half-life of various reporter transcripts in the presence of actinomycin D

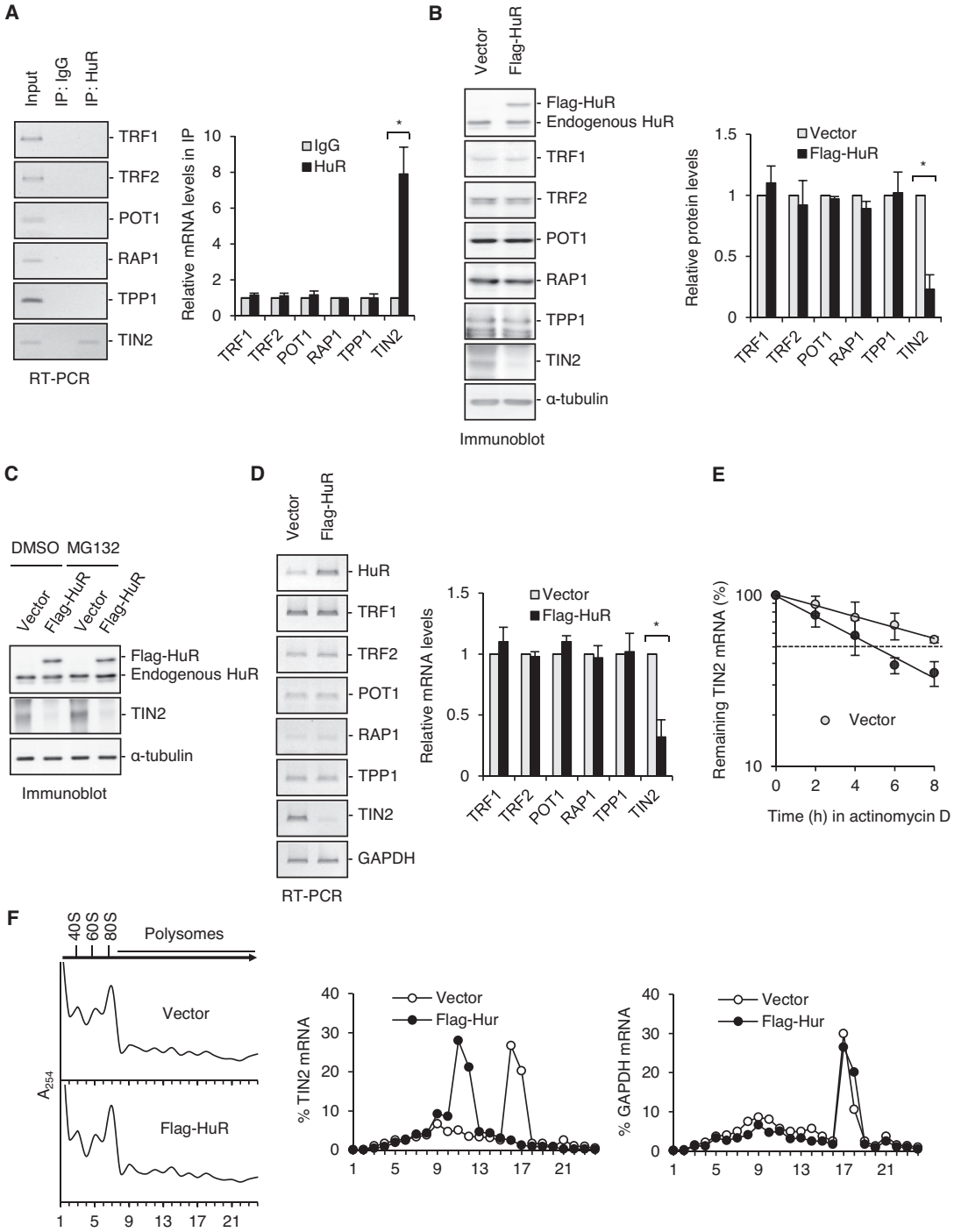

Figure 1. HuR represses TIN2 expression by destabilizing *TIN2* mRNA and reducing its translation. (**A**) HeLa cell lysates were subjected to immunoprecipitation (IP) with anti-HuR antibody, followed by quantitative RT-PCR to measure the enrichment of mRNAs of shelterin proteins in HuR IP compared with control IgG IP. Graphical representation of the relative mRNA levels of shelterin proteins in HuR IP normalized against the IgG control. (**B**) HeLa cells expressing Flag-HuR were analyzed by immunoblot analysis to detect various shelterin proteins and used α-tubulin as a loading control. Graphical representation of the relative levels of shelterin proteins normalized against the vector control. (**C**) HeLa cells expressing Flag-HuR were treated with 10 mM MG132 for 6 h and analyzed by immunoblot with antibodies against HuR and TIN2. (**D**) HeLa cells expressing Flag-HuR were analyzed by quantitative RT-PCR to detect the mRNA levels of various shelterin proteins. Graphical representation of the relative levels of shelterin mRNAs normalized against the vector control. (**E**) HeLa cells were transfected with Flag-HuR and treated with 2 μg/ml actinomycin D for the indicated periods. Total RNA was extracted at each time point, and the *TIN2* mRNA levels were measured by quantitative real-time PCR and normalized against the *GAPDH* mRNA. The results represent the average of three independent experiments. (**F**) HeLa cells expressing Flag-HuR were fractionated into cytoplasmic extracts through sucrose gradients. The arrow indicates the direction of sedimentation. Small (40S) and large (60S) ribosomal subunits, monosomes (80S), and larger polysomes are shown from low to high molecular weights. The distribution of *TIN2* and *GAPDH* mRNAs was quantified by RT-PCR analysis of RNA isolated from 24 gradient fractions. The histograms represent the means and standard errors of the means from three independent experiments. Statistical analyses were performed using a two-tailed, equal-sample variance Student's *t*-test. $*P < 0.001$.

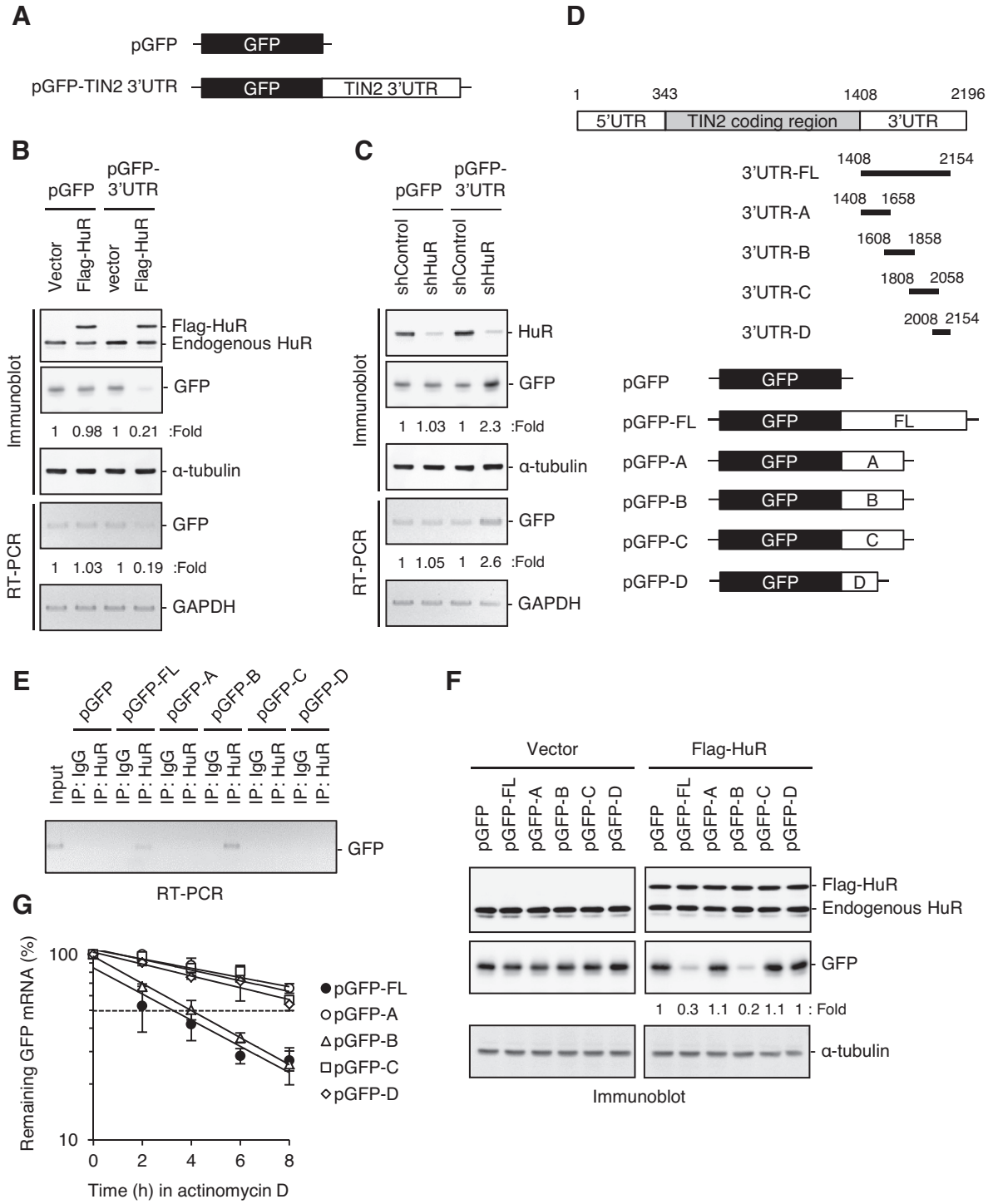

Figure 2. HuR represses TIN2 expression through interaction with the TIN2 3′UTR. (**A**) Plasmid pGFP-TIN2 3′UTR was constructed by linking the entire TIN2 3′UTR after the GFP coding region. (**B**) HeLa cells were transfected with pGFP-TIN2 3′UTR or pGFP together with Flag-HuR and analyzed by immunoblot to assess the levels of reporter GFP protein and HuR. The relative levels of GFP protein were normalized against the loading control α-tubulin. The mRNA levels of GFP and GFP-TIN2 3′UTR were measured by quantitative RT-PCR and normalized against *GAPDH* mRNA. (**C**) HeLa cells were transfected with pGFP-TIN2 3′UTR or pGFP together with HuR shRNA (shHuR) or control shRNA (shControl), and analyzed by immunoblot to measure the levels of reporter GFP protein and HuR, and by quantitative RT-PCR to detect the mRNA levels of GFP and GFP-TIN2 3′UTR. (**D**) Constructs were prepared to express chimeric RNAs spanning the GFP coding region and each of the four TIN2 3′UTR segments. (**E**) HeLa cells expressing GFP or GFP-TIN2 3′UTR segments were subjected to immunoprecipitation with anti-HuR antibody, followed by quantitative RT-PCR to measure the enrichment of *GFP* mRNA in HuR IP compared with control IgG IP. (**F**) HeLa cells were transfected with pGFP-TIN2 3′UTR segments together with Flag-HuR and analyzed by immunoblot to detect reporter GFP protein and HuR. The relative levels of GFP protein were normalized against the loading control α-tubulin. (**G**) HeLa cells were transfected with pGFP-TIN2 3′UTR segments and treated with 2 μg/ml actinomycin D for the indicated periods. The *GFP* mRNA levels were measured by quantitative real-time PCR and normalized against the *GAPDH* mRNA. The results represent the average of three independent experiments.

and found that HuR reduced the half-life of GFP-FL and GFP-B transcripts (Figure 2G). Because fragment B is still quite long (~250 bp), we mapped the interaction of HuR in fragment B in closer detail. As shown in Supplementary Figure S5, the first 50 bp of fragment B is responsible for HuR-dependent repression of GFP.

Depletion of HuR levels enhances TIN2 expression and induces growth arrest

Given that HuR levels decline during replicative senescence in human fibroblasts (39–42), we examined whether HuR depletion is sufficient to induce senescence in HeLa cells. To address this issue, we infected HeLa cells with retrovirus particles expressing two different shRNAs that inhibit HuR expression (shHuR-1 and shHuR-2) or control shRNA (shControl). Stable cell lines were established as mass cultures from separate transductions and monitored population doubling (PD) at regular intervals. HuR knockdown cells maintained reduced levels of HuR throughout the duration of the experiments (see Figure 3C). The growth rates of two independent HuR knockdown cell lines gradually slowed down and almost stopped dividing at ~PD 50 (Figure 3A). We next examined whether this growth arrest correlates with an altered cell cycle distribution. HuR knockdown cells exhibited an increase in the proportion of cells in G1 and a concomitant decrease in the proportion of cells in S, G2, and M phases, which is consistent with growth arrest in the G1 phase of the cell cycle (Figure 3B). In addition, HuR knockdown cells at PD 42 showed increased levels of p53, $p21^{Cip1}$, and $p16^{INK4a}$, which indicates cellular senescence (Figure 3C) (53–55). In contrast, these senescence-associated genes were not induced at PD 3. HuR knockdown cells were also stained intensely for SA-β-Gal activity at PD 42 and displayed a flattened and enlarged morphology (Supplementary Figure S6). These results suggest that HuR is essential for cell proliferation in HeLa cells.

Because HuR decreases TIN2 protein levels by destabilizing *TIN2* mRNA and reducing its translation, we examined whether converse HuR depletion increases TIN2 expression. HuR knockdown cells maintained elevated levels of TIN2 protein throughout the duration of the experiments, but did not alter the levels of other shelterin proteins (Figure 3D). The levels of *TIN2* mRNA were also increased in HuR knockdown cells compared to control cells, as measured by RT-PCR analysis (Figure 3E). We also measured the half-life of *TIN2* mRNA by treating cells with actinomycin D. The half-life of *TIN2* mRNA was prolonged by HuR depletion (Figure 3F), further supporting our hypothesis that HuR reduces the stability of *TIN2* mRNA. In contrast, the half-life of TIN2 protein was not influenced by HuR depletion (Supplementary Figure S7), indicating that HuR does not affect the stability of TIN2 protein.

We next examined whether the levels of TIN2 are also elevated in human fibroblasts rendered senescent phenotype via replicative exhaustion. As shown in Supplementary Figure S8, IMR90 fibroblasts exhibited growth arrest at ~PD 55 by replicative senescence. Whereas HuR protein levels were decreased as cells entered senescence, TIN2 protein levels were markedly increased in senescent cells compared to young cells, but the levels of other shelterin proteins were not altered. These findings support the idea that HuR negatively regulates the levels of TIN2 during normal replicative senescence.

Telomere dysfunction can result in telomere dysfunction-induced foci (TIFs) by activation of a DNA damage response at telomeres (56,57). Moreover, telomeres are favored targets of a persistent DNA damage response in cellular senescence (58). Because HuR depletion increases the levels of TIN2 protein, we tested whether HuR depletion induces TIFs in the nucleus. The TIFs identified with 53BP1 (Figure 3G) and γH2AX (Supplementary Figure S9) antibodies were examined in HuR knockdown and shRNA control cells. Although TIN2 expression was increased immediately upon HuR depletion, TIFs were not induced by HuR depletion at PD 3, suggesting that the increase in TIN2 caused by HuR depletion had no direct effect on telomere maintenance. Intriguingly, depletion of HuR induced numerous 53BP1 and γH2AX foci at telomeres when cells entered cellular senescence (at PD 42). Approximately 60% of HuR knockdown cells contained more than five TIFs per nucleus (Figure 3H). These results suggest that induction of TIFs could be a senescence-associated phenotype, but not directly due to TIN2 overexpression.

Because HuR depletion leads to cellular senescence, we investigated the effect of HuR depletion on the regulation of telomere length. We measured telomere length by telomere quantitative fluorescence *in situ* hybridization (Q-FISH). Relative telomere lengths were not altered even when HuR knockdown cells were at late PDs (Supplementary Figure S10), suggesting that HuR depletion-induced growth arrest is not caused by telomere shortening in HeLa cells.

Depletion of HuR increases mitochondrial localization of TIN2, but does not affect TIN2 nuclear localization

Given that TIN2, in addition to being localized to telomeres, can also be targeted to the mitochondria by its N-terminal mitochondrial targeting sequence (23), we examined the effect of HuR depletion on subcellular localization of TIN2 in HuR knockdown cells. Endogenous TIN2 exhibited a punctate staining pattern in the nucleus and also localized to the cytoplasm (Figure 4A). The cytoplasmic staining of TIN2 overlapped with the mitochondrial marker TOM20, indicating mitochondrial targeting of TIN2. We noticed that the cytoplasmic TIN2 signals appeared to be slightly higher in HuR knockdown cells than in control cells. However, TIN2 signals colocalized with telomeres in the nucleus were not altered by HuR depletion. These results suggest that the increase in TIN2 caused by HuR depletion may be confined to the mitochondria.

To further investigate TIN2 subcellular distribution, we separately collected nuclear, soluble cytoplasmic, and heavy membrane protein fractions from control and HuR knockdown cells. Successful fractionation was indicated by the relative enrichment of the respective proteins in various fractions, and mitochondria were enriched as expected in the heavy membrane fraction. Consistent with the immunofluorescence results, a clear increase in TIN2 levels was observed in the mitochondrial fraction of HuR knockdown cells, whereas TIN2 levels in the nuclear fraction were not affected by HuR depletion (Figure 4B). On the other

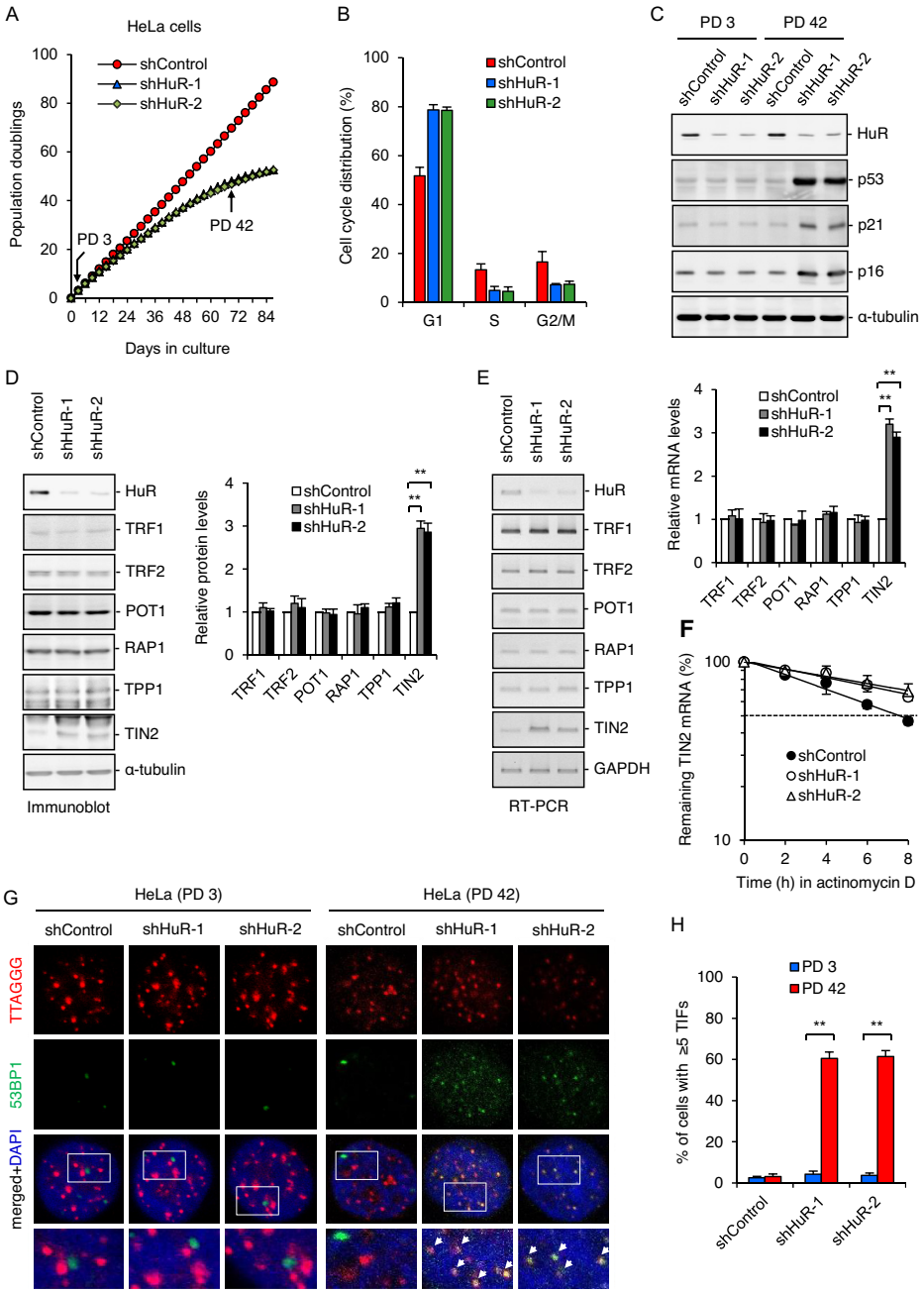

Figure 3. Depletion of HuR enhances TIN2 expression and induces cellular senescence. (**A**) Cell growth curves of HeLa cells stably expressing control shRNA (shControl) or HuR shRNAs (shHuR-1 and shHuR-2). Stable cells were replated every 3–4 days to maintain log-phase growth and calculate the growth rate, with day 0 representing the first day after puromycin selection. (**B**) Cell cycle profiles of stable clones expressing control shRNA or HuR shRNAs. Stable cells were harvested at PD 42 after selection, and cell cycle profiles were determined by propidium iodide staining and flow cytometry. The results represent the average of three independent experiments. (**C**) Stable cells expressing control shRNA or HuR shRNAs were harvested at the indicated PDs and analyzed by immunoblot to measure the protein levels of HuR, p53, p21, and p16. (**D**) Stable cells expressing control shRNA or HuR shRNAs were harvested at PD 42 and analyzed by immunoblot to detect various shelterin proteins. Graphical representation of the relative levels of shelterin proteins normalized against the control shRNA. (**E**) Stable cells expressing control shRNA or HuR shRNAs were harvested at PD 42 and analyzed by quantitative RT-PCR to measure the mRNA levels of various shelterin proteins. Graphical representation of the relative levels of shelterin mRNAs normalized against the control shRNA. (**F**) Stable cells expressing control shRNA or HuR shRNAs were treated with 2 μg/ml actinomycin D for the indicated periods. The *TIN2* mRNA levels were measured by quantitative real-time PCR and normalized against the *GAPDH* mRNA. The results represent the average of three independent experiments. (**G**) Stable cells expressing control shRNA or HuR shRNAs at the indicated PDs were analyzed by indirect immunofluorescence for co-localization of 53BP1 foci (green) with telomeric sites marked by TTAGGG-specific FISH probe (red). DNA was stained with DAPI (blue). A subset of 53BP1 foci colocalized with TTAGGG probe are indicated by arrows. (**H**) Quantification of the induction of TIFs by HuR depletion. Cells with five or more DNA-damage foci colocalized with TTAGGG probe were scored as TIF positive. For each condition, at least 100 nuclei were counted. The histograms represent the means and standard errors of the means from three independent experiments. Statistical analyses were performed using a two-tailed, equal-sample variance Student's *t*-test. $^{**}P < 0.0001$.

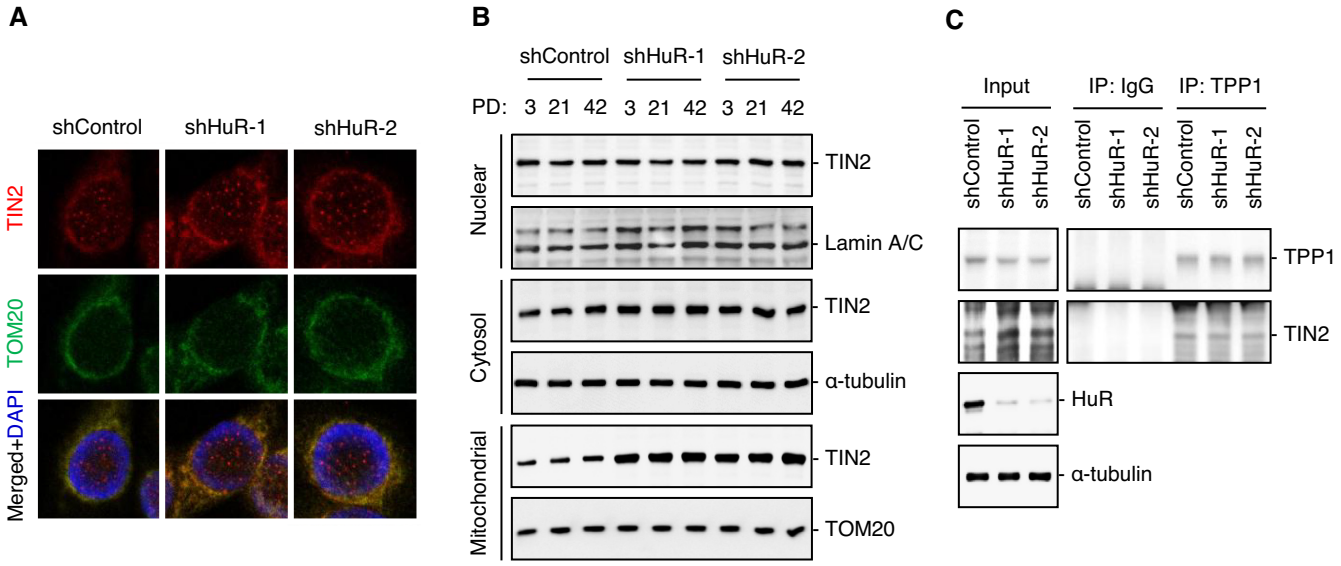

Figure 4. Depletion of HuR increases mitochondrial localization of TIN2. (**A**) HeLa cells stably expressing control shRNA or HuR shRNAs were analyzed by indirect immunofluorescence for co-localization of TIN2 with TOM20 (mitochondrial marker). DNA was stained with DAPI. (**B**) Stable cells expressing control shRNA or HuR shRNAs were harvested at the indicated PDs. Nuclear, cytosolic, and mitochondrial fractions were separately collected and analyzed by immunoblot with anti-TIN2 antibodies. Blots were immunolabeled with anti-lamin (for nuclear fraction), anti-tubulin (for cytosolic fraction), and anti-TOM20 (for mitochondrial fraction) antibodies as loading controls. (**C**) Stable cells expressing control shRNA or HuR shRNAs were subjected to immunoprecipitation with anti-TPP1 antibodies, followed by immunoblot analysis with anti-TIN2 antibodies. IgG was used as a negative control.

hand, the cytoplasmic levels of TIN2 are slightly increased in HuR knockdown cells compared to control cells. This could be due to enhanced expression of TIN2 caused by HuR depletion. These results suggest that increased TIN2 levels occur in the mitochondria. We noticed that HuR knockdown cells maintained the increased mitochondrial localization of TIN2 until PD 42 (Figure 4B).

It has been reported that a TIN2-TPP1 interaction is important for targeting TIN2 to the nucleus (25). Disruption of the TPP1-interacting region in TIN2 resulted in decreased nuclear localization of TIN2 (23). To test whether HuR depletion affects the interaction between TIN2 and TPP1, we performed immunoprecipitation analysis with anti-TPP1 antibodies in HuR knockdown cells. The amounts of TIN2 in anti-TPP1 immunoprecipitates were not altered by HuR depletion (Figure 4C), indicating that HuR depletion did not affect TIN2 nuclear localization.

Depletion of HuR results in high levels of ROS through mitochondrial targeting of TIN2

TIN2 has been reported to regulate mitochondrial oxidative phosphorylation (23). Reducing TIN2 expression enhanced ATP and oxygen production, and inhibited ROS generation. Given that HuR depletion enhances mitochondrial localization of TIN2, HuR depletion may lead to an increase in ROS levels possibly due to TIN2 mitochondrial targeting. Consequently, elevating mitochondrial ROS levels could contribute to the induction and maintenance of cellular senescence. To test this hypothesis, we examined the impact of HuR depletion on ROS production. HuR knockdown and control cells were analyzed for mitochondrial superoxide levels at early and late PDs using MitoSOX Red and flow cytometry. Mitochondrial superoxide levels were slightly higher in HuR knockdown cells than in control cells at PD 3 and further enhanced at PD 42 (Figure 5A). We also explored the effect of the mitochondrial ROS scavenger MitoTempo in HuR knockdown cells. The increase in mitochondrial superoxide levels was prevented by the treatment of MitoTempo (Figure 5B). To further verify the HuR depletion-mediated increase in superoxide levels, we performed the fluorescence detection analysis using confocal microscopy. Consistent with the flow cytometry results, MitoSOX Red signals in HuR knockdown cells were higher than in control cells at PD 3 and further enhanced at PD 42 (Figure 5C). Taken together, these results indicate that HuR depletion causes increased mitochondrial ROS levels as the cells enter senescence.

To determine whether the increase in ROS levels caused by HuR depletion is directly due to increased TIN2 expression, HeLa cells were transiently transfected with TIN2-Myc and analyzed for mitochondrial ROS levels. We used TIN2 tagged with Myc on the C terminus, as N-terminal tagging blocks TIN2 mitochondrial localization (23). Mitochondrial ROS levels were increased in TIN2-expressing cells compared to control cells (Figure 5D), which was further verified by MitoSOX RED fluorescence detection (Figure 5E). These results imply that TIN2 contributes, at least in part, to the induction of cellular senescence by elevating the basal levels of oxidative stress.

As the cancer cell lines are genetically altered, we wanted to confirm the above data in a human primary fibroblast IMR90 cell line. IMR90 cells were infected at early PD with retrovirus particles expressing HuR or control shRNA. As shown in Supplementary Figure S10A, depletion of HuR induced cellular senescence at ∼ PD 30, whereas control cells exhibited growth arrest at ∼PD 55. As in HeLa cells, mitochondrial ROS levels were induced by HuR depletion

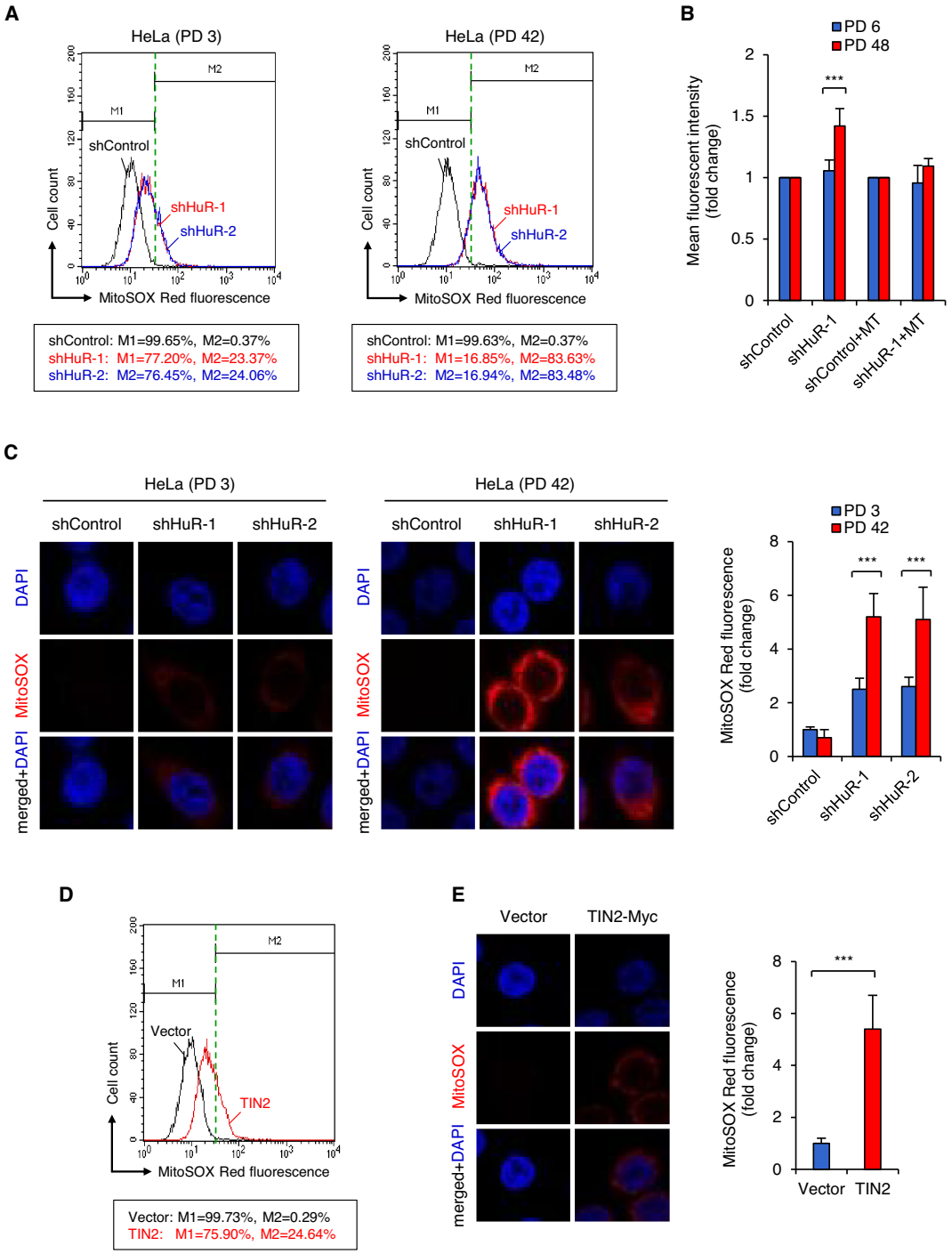

Figure 5. Depletion of HuR increases the ROS levels through enhanced mitochondrial targeting of TIN2. (**A**) HeLa cells stably expressing control shRNA or HuR shRNAs at the indicated PDs were incubated with 5 μM MitoSOX Red and analyzed for detection of the mitochondrial superoxide levels by flow cytometry. Results were presented by 'M1 and M2 percentage' fluorescence variation. M1 is placed around the control cells, and M2 is placed to the right of M1 to indicate an increase in ROS level. (**B**) Stable cells expressing control shRNA or HuR shRNAs at the indicated PDs were incubated with or without 10 μM MitoTempo (MT) for 2 h. Harvested cells were incubated with 5 μM MitoSOX Red, and the mitochondrial superoxide levels were presented as the mean fluorescent intensity fold change compared to the average value of control. (**C**) Stable cells expressing control shRNA or HuR shRNAs at the indicated PDs were incubated with 5 μM MitoSOX Red and analyzed for fluorescence detection of the mitochondrial superoxide levels. Digital images of MitoSOX Red fluorescence were obtained by confocal microscopy and overlaid on the DAPI images. ROS levels are presented as the mean fluorescence intensity fold change compared to the average value of control. (**D**) HeLa cells transfected with TIN2-Myc were incubated with 5 μM MitoSOX and analyzed for detection of the mitochondrial ROS levels by flow cytometry. Results were presented by 'M1 and M2 percentage' fluorescence variation. (**E**) HeLa cells transfected with TIN2-Myc were incubated with 5 μM MitoSOX Red and analyzed for fluorescence detection of the mitochondrial ROS levels. Digital images of MitoSOX Red fluorescence were obtained by confocal microscopy and overlaid with DAPI images. ROS levels are presented as the mean fluorescence intensity fold change compared to the average value of control. The histograms represent the means and standard errors of the means from three independent experiments. Statistical analyses were performed using a two-tailed, equal-sample variance Student's *t*-test. ***$P < 0.005$.

at early passage and further increased at later passage (Supplementary Figure S11B and C). We also found that overexpression of TIN2-Myc caused an increase in mitochondrial ROS levels (Supplementary Figure S11D and E). Therefore, HuR depletion-induced ROS production could be due to TIN2 overexpression, but not related to specific cell line backgrounds.

Mitochondrial localization of TIN2 leads to increased ROS levels

TIN2 contains two potential amphipathic helices within the N-terminal first 90 residues, which are essential and sufficient to target TIN2 to mitochondria (23). Mutations at F37D/L38E or L48E within this region enhance mitochondrial targeting and inhibit nuclear localization by disrupting TIN2 interaction with TPP1 (23). Conversely, mutations at K62A/K64A reduce mitochondrial localization and maintain TPP1 binding ability to TIN2 (23). To examine the effects of these mutations on TIN2 subcellular localization, we transfected HeLa cells with wild-type or mutant TIN2-Myc expression vectors and subjected them to immunofluorescence staining. Wild-type TIN2 was detected in both the nucleus and the cytoplasm. The cytoplasmic signals overlapped with the mitochondrial marker TOM20 (Figure 6A). When co-expressed with Flag-TPP1, TIN2 was predominantly localized to the nucleus, supporting the notion that TPP1 binding causes TIN2 to accumulate in the nucleus. The F37D/L38E and L48E mutants predominantly localized to the mitochondria, whereas the majority of the K62A/K64A mutant proteins were detected in the nucleus (Figure 6A). Consistent with previous report (23), TIN2 was found to be proteolytically processed into the shorter fragments in the mitochondria (Figure 6B). Under the conditions in which nuclear localization of TIN2 was favored, mitochondrial processing was diminished.

We next investigated whether mitochondria-targeted TIN2 increases ROS levels. Because TIN2 translocation to the mitochondria is inhibited by TPP1 binding, we transfected HeLa cells with wild-type and mutant TIN2-Myc together with or without Flag-TPP1, and assessed for mitochondrial ROS levels. Whereas overexpression of wild-type TIN2 alone slightly enhanced mitochondrial ROS levels compared to the vector control, co-expression of TPP1 significantly attenuated ROS production (Figure 6C). The F37D/L38E and L48E mutant cells exhibited higher ROS levels in the mitochondria regardless of TPP1 expression, whereas the K62A/K64A mutant cells maintained only basal levels of ROS (Figure 6C). Similar results were obtained by fluorescence detection using confocal microscopy (Supplementary Figure S12). These findings demonstrate that mitochondria-targeted TIN2 causes an increase in ROS levels.

Because the F37D/L38E and L48E mutants show higher ROS levels in the mitochondria, we examined whether stable expression of these mutants in HeLa cell may induce growth suppression. HeLa cell lines stably expressing wild-type TIN2 or K62A/K64A grew normally and continued to divide throughout the duration of the experiments (Figure 6D). In contrast, the growth rates of cells stably expressing F37D/L38E or L48E mutants gradually slowed down and almost stopped dividing at ∼PD 35. This growth arrest was accompanied by altered cell cycle distribution (Figure 6E) and enhanced expression of senescence-associated genes at late PD (Figure 6F). About 70% of F37D/L38E- or L48E-expressing cells were stained intensely for SA-β-Gal activity, and displayed a flattened and enlarged morphology (Supplementary Figure S13). However, no such changes were found in cells expressing wild-type TIN2 and K62A/K64A. Overexpression of F37D/L38E or L48E led to an increase in mitochondrial ROS levels (Figure 6G), which was further verified by MitoSOX RED fluorescence detection (Supplementary Figure S14). Taken together, these results suggest that high ROS production is a direct result of mitochondrial targeting of TIN2.

DISCUSSION

HuR protein regulates the stability, translation, and intracellular localization of various mRNAs. However, the biological consequence of HuR association varies depending on its target mRNA (26–30). Although the underlying mechanisms are not fully understood, HuR has been shown to stabilize target mRNAs that encode proteins associated with cell proliferation and cell cycle progression (40). Given that HuR levels decreases with replicative senescence, the expression levels of these target mRNAs are reduced in senescent cells. Conversely, loss of HuR during replicative senescence leads to stabilization of mRNAs encoding cell growth-inhibitory proteins (38). Since progressive telomere loss leads to replicative senescence by limiting the replicative capacity of dividing cells (59), we explored the influence of HuR on the expression of shelterin proteins. Here we show that HuR decreases TIN2 protein levels by destabilizing *TIN2* mRNA and reducing its translation. Depletion of HuR enhances mitochondrial targeting of TIN2, subsequently leading to an increase in ROS levels, which in turn contributes to induction of cellular senescence. These findings provide compelling evidence for a novel role of HuR in controlling the process of cell growth and cellular senescence.

Among the six shelterin transcripts, HuR associates with and destabilizes the 3′UTR of *TIN2* mRNA. HuR association is specific for TIN2, as HuR did not affect the mRNA levels of other shelterin proteins. This association was further confirmed using GFP-derived reporter constructs. The critical question that remains to be answered is how HuR destabilizes *TIN2* mRNA. The mechanism may involve the recruitment of the RNA-induced silencing complex (RISC) through the direct interaction of RISC with HuR on *TIN2* mRNA. For instance, HuR and AUF1 have been shown to directly associate with the 3′UTR of *p16* mRNA, and this association was proposed to recruit RISC to mRNA, thereby destabilizing it (38). Because the knockdown of either HuR or AUF1 increases p16 expression, these two different RNA-binding proteins represses p16 expression through an interdependent mechanism. In the case of c-Myc, association of HuR with mRNA adjacent to the let-7 binding site facilitates the recruitment of let-7-loaded RISC, resulting in repression of c-Myc expression (37). This indicates that HuR and miRNA can function jointly to regulate target mRNA stability. These findings

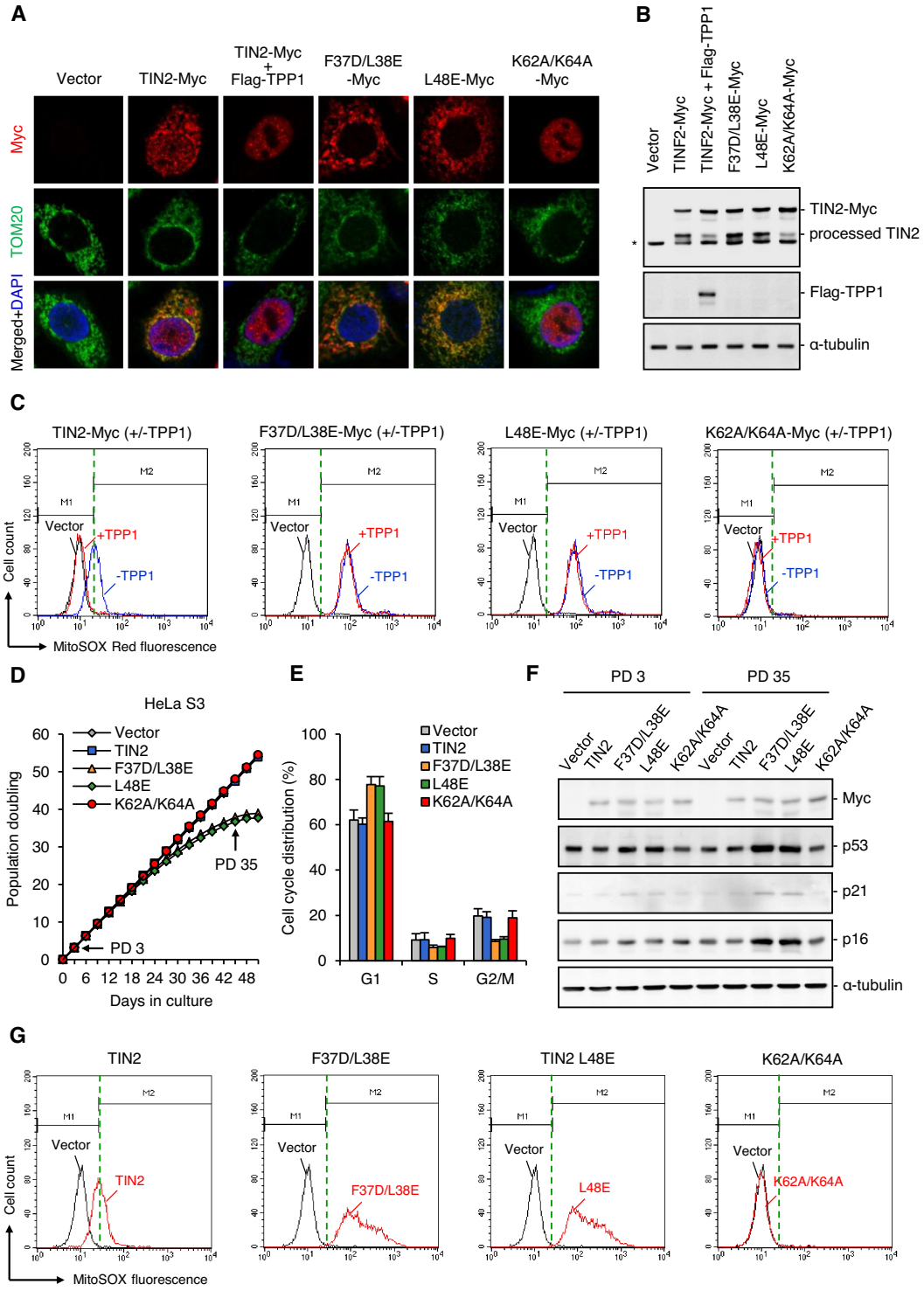

Figure 6. Mitochondrial targeting of TIN2 leads to enhanced ROS levels. (**A**) HeLa cells were transfected with wild-type and mutant TIN2-Myc together with Flag-TPP1 as indicated and analyzed by indirect immunofluorescence for co-localization of TIN2 with TOM20 (mitochondrial marker). (**B**) HeLa cells were transfected with wild-type and mutant TIN2-Myc together with Flag-TPP1 and analyzed by immunoblot with anti-Myc and anti-Flag antibodies. The *asterisk* marks the position of nonspecific bands. (**C**) HeLa cells were transfected with wild-type and mutant TIN2-Myc together with Flag-TPP1, incubated with 5 μM MitoSOX, and analyzed for detection of the mitochondrial ROS levels by flow cytometry. Results were presented by 'M1 and M2 percentage' fluorescence variation. (**D**) Cell growth curves of HeLa cells stably expressing wild-type and mutant TIN2-Myc proteins. Stable cells were replated every 3–4 days to maintain log-phase growth and calculate the growth rate. (**E**) Stable cells expressing wild-type and mutant TIN2-Myc proteins were harvested at PD 35, and cell cycle profiles were determined by propidium iodide staining and flow cytometry. The results represent the average of three independent experiments. (**F**) Stable cells expressing wild-type and mutant TIN2-Myc proteins were harvested at the indicated PDs and analyzed by immunoblot to measure the protein levels of p53, p21 and p16. (**G**) Stable cells expressing wild-type and mutant TIN2-Myc proteins at PD 35 were incubated with 5 μM MitoSOX and analyzed for detection of the mitochondrial ROS levels by flow cytometry.

suggest that RISC-mediated regulation might be a common mechanism in HuR-dependent destabilization of target mRNAs. It will be of immediate interest to investigate the involvement of miRNA and other RNA-binding proteins in HuR-dependent *TIN2* mRNA regulation.

Nuclear TIN2 plays an essential role in the structural integrity of shelterin by connecting the TPP1/TOP1 heterodimer to TRF1 and TRF2 on the duplex telomeric repeats (7,8). In this study, we demonstrate that HuR depletion increases mitochondrial translocation of TIN2. TIN2 translocation to the mitochondria was abrogated by overexpression of TPP1, which is consistent with previous report that TIN2-TPP1 interaction in the cytoplasm is important for targeting TIN2 to the nucleus (23). These observations indicate that TIN2 has dual localizations and regulates mitochondrial function independent of its role in the telomere. The important biological consequence of mitochondrial targeting of TIN2 is the production of ROS. Overexpression of wild-type TIN2 enhances the mitochondrial ROS levels, but co-expression of TPP1 significantly attenuated ROS. In addition, expression of the F37D/L38E and L48E mutants, which enhance mitochondrial localization, leads to constitutive production of high ROS levels. However, expression of K62A/K64A mutant, which inhibits mitochondrial translocation, results in reduced ROS levels. Based on our data presented in this study, we propose the following model to explain the mechanism by which reduced HuR levels contribute to induction and maintenance of cellular senescence. In this model, low HuR expression contributes to accumulating TIN2 in the mitochondria, which in turn maintains the high levels of ROS, leading to induction of cellular senescence. On the other hand, high HuR expression in dividing cells represses TIN2 expression and decreases its mitochondrial translocation, thereby maintaining a highly proliferative state. Our model supports the finding that HuR has been found to be highly expressed in numerous cancers (60,61). Since HuR stabilizes the proliferative transcripts and destabilizes the growth-inhibitory transcripts, aberrant expression of HuR could cause normal cell transformation.

The effects of HuR on cellular senescence are not caused by telomere dysfunction, but rather by TIN2's presence in the mitochondria. This conclusion is based on the following pieces of data. First, loss of HuR during cellular senescence did not affect nuclear localization of TIN2. Second, although loss of telomere length can induce human replicative senescence, we did not observe any change in telomere length during HuR depletion-induced senescence in HeLa cells. Third, telomere dysfunction was not induced in TIN2-overexpressing cells, as determined by TIF analysis (Supplementary Figure S15). Finally, mitochondrial localization of TIN2 led to an increase in ROS levels, resulting in induction of cellular senescence. Thus, we conclude that HuR-mediated cellular senescence is a direct result of the mitochondrial targeting of TIN2 initiated by HuR depletion.

It is well documented that ROS produced by mitochondria contributes to induction of cellular senescence (62,63). Lowering the levels of intracellular antioxidants accelerates the premature onset of senescence, while increasing cellular oxidant scavengers appears to delay senescence. Although HuR expression is reduced in human fibroblasts during replicative senescence and in aged human tissues (39–42), the mechanism by which HuR regulates ROS levels is not yet fully understood. Through regulation of the turnover and/or translation of various target mRNAs, HuR could possibly diminish ROS levels by either reducing ROS production or by enhancing ROS clearance. Although our findings highlight the HuR-TIN2 regulatory axis as a critical regulator of cellular oxidative stress, other HuR targets may also contribute to regulation of mitochondria-derived ROS. Recently, Zarei *et al.* demonstrated that HuR enhances antioxidant activity of pancreatic cancer cells by upregulating a NADPH-generating enzyme, isocitrate dehydrogenase 1 (IDH1) (64). Thus, multiple pathways could be involved in controlling mitochondrial ROS levels by prosurvival protein, HuR. Recent research progress has indicated that TERT is localized to the mitochondria and alleviates intracellular ROS production in a telomere-independent way (65). In this work, we found that HuR does not interact with mRNAs encoding telomerase holoenzyme components including TERT (Supplementary Figure S1). These results suggest that telomerase activity and TERT localization could not be affected by HuR protein.

Although our findings in this work support a role for ROS in mediating cellular senescence, important question remains as to how mitochondrial targeting of TIN2 leads to increased ROS levels. One possible mechanism is that HuR-dependent TIN2 activation may induce the electron leak from the electron transport chain, leading to a higher rate of ROS production in the mitochondria, although the underlying signaling remains elusive. Alternatively, TIN2 may associate with intracellular antioxidant enzymes such as superoxide dismutase and catalase and inhibit their enzymatic activity, leading to a rise in intracellular ROS levels. Based on our findings presented herein, further investigation of the role of mitochondrial TIN2 in the onset of cellular senescence will provide a useful therapeutic route for modulating intracellular ROS levels in both aging and cancer.

SUPPLEMENTARY DATA

Supplementary Data are available at NAR Online.

ACKNOWLEDGEMENTS

We thank Dr Sang-Jun Ha and Myeong Joon Kim for technical help, and the Chung lab members for constructive suggestions and thoughtful critiques of the work.

FUNDING

National Research Foundation of Korea [NRF-2013M3A9B6076431, NRF-2016R1A5A1010764 to I.K.C.]; Yonsei University Intramural Research [2014-22-0096 to I.K.C.]. Funding for open access charge: National Research Foundation of Korea.
Conflict of interest statement. None declared.

REFERENCES

1. Blackburn,E.H. (2001) Switching and signaling at the telomere. *Cell*, **106**, 661–673.

2. Smogorzewska,A. and de Lange,T. (2004) Regulation of telomerase by telomeric proteins. *Annu. Rev. Biochem.*, **73**, 177–208.
3. Liu,D., O'Connor,M.S., Qin,J. and Songyang,Z. (2004) Telosome, a mammalian telomere-associated complex formed by multiple telomeric proteins. *J. Biol. Chem.*, **279**, 51338–51342.
4. de Lange,T. (2005) Shelterin: the protein complex that shapes and safeguards human telomeres. *Genes Dev.*, **19**, 2100–2110.
5. Palm,W. and de Lange,T. (2008) How shelterin protects mammalian telomeres. *Annu. Rev. Genet.*, **42**, 301–334.
6. Sfeir,A. and de Lange,T. (2012) Removal of shelterin reveals the telomere end-protection problem. *Science*, **336**, 593–597.
7. Kim,S.H., Beausejour,C., Davalos,A.R., Kaminker,P., Heo,S.J. and Campisi,J. (2004) TIN2 mediates functions of TRF2 at human telomeres. *J. Biol. Chem.*, **279**, 43799–43804.
8. Ye,J.Z., Donigian,J.R., van Overbeek,M., Loayza,D., Luo,Y., Krutchinsky,A.N., Chait,B.T. and de Lange,T. (2004) TIN2 binds TRF1 and TRF2 simultaneously and stabilizes the TRF2 complex on telomeres. *J. Biol. Chem.*, **279**, 47264–47271.
9. Ye,J.Z., Hockemeyer,D., Krutchinsky,A.N., Loayza,D., Hooper,S.M., Chait,B.T. and de Lange,T. (2004) POT1-interacting protein PIP1: a telomere length regulator that recruits POT1 to the TIN2/TRF1 complex. *Genes Dev.*, **18**, 1649–1654.
10. Liu,D., Safari,A., O'Connor,M.S., Chan,D.W., Laegeler,A., Qin,J. and Songyang,Z. (2004) PTOP interacts with POT1 and regulates its localization to telomeres. *Nat. Cell Biol.*, **6**, 673–680.
11. Lei,M., Podell,E.R. and Cech,T.R. (2004) Structure of human POT1 bound to telomeric single-stranded DNA provides a model for chromosome end-protection. *Nat. Struct. Mol. Biol.*, **11**, 1223–1229.
12. Kim,S.H., Davalos,A.R., Heo,S.J., Rodier,F., Zou,Y., Beausejour,C., Kaminker,P., Yannone,S.M. and Campisi,J. (2008) Telomere dysfunction and cell survival: roles for distinct TIN2-containing complexes. *J. Cell Biol.*, **181**, 447–460.
13. Takai,K.K., Kibe,T., Donigian,J.R., Frescas,D. and de Lange,T. (2011) Telomere protection by TPP1/POT1 requires tethering to TIN2. *Mol. Cell*, **44**, 647–659.
14. Zhong,F.L., Batista,L.F., Freund,A., Pech,M.F., Venteicher,A.S. and Artandi,S.E. (2012) TPP1 OB-fold domain controls telomere maintenance by recruiting telomerase to chromosome ends. *Cell*, **150**, 481–494.
15. Xin,H., Liu,D., Wan,M., Safari,A., Kim,H., Sun,W., O'Connor,M.S. and Songyang,Z. (2007) TPP1 is a homologue of ciliate TEBP-beta and interacts with POT1 to recruit telomerase. *Nature*, **445**, 559–562.
16. Nandakumar,J., Bell,C.F., Weidenfeld,I., Zaug,A.J., Leinwand,L.A. and Cech,T.R. (2012) The TEL patch of telomere protein TPP1 mediates telomerase recruitment and processivity. *Nature*, **492**, 285–289.
17. Abreu,E., Aritonovska,E., Reichenbach,P., Cristofari,G., Culp,B., Terns,R.M., Lingner,J. and Terns,M.P. (2010) TIN2-tethered TPP1 recruits human telomerase to telomeres in vivo. *Mol. Cell. Biol.*, **30**, 2971–2982.
18. Sexton,A.N., Regalado,S.G., Lai,C.S., Cost,G.J., O'Neil,C.M., Urnov,F.D., Gregory,P.D., Jaenisch,R., Collins,K. and Hockemeyer,D. (2014) Genetic and molecular identification of three human TPP1 functions in telomerase action: recruitment, activation, and homeostasis set point regulation. *Genes Dev.*, **28**, 1885–1899.
19. Calado,R.T. and Young,N.S. (2009) Telomere diseases. *N. Engl. J. Med.*, **361**, 2353–2365.
20. Du,H.Y., Mason,P.J., Bessler,M. and Wilson,D.B. (2009) TINF2 mutations in children with severe aplastic anemia. *Pediatr. Blood Cancer*, **52**, 687.
21. Sasa,G.S., Ribes-Zamora,A., Nelson,N.D. and Bertuch,A.A. (2012) Three novel truncating TINF2 mutations causing severe dyskeratosis congenita in early childhood. *Clin. Genet.*, **81**, 470–478.
22. Savage,S.A., Giri,N., Baerlocher,G.M., Orr,N., Lansdorp,P.M. and Alter,B.P. (2008) TINF2, a component of the shelterin telomere protection complex, is mutated in dyskeratosis congenita. *Am. J. Hum. Genet.*, **82**, 501–509.
23. Chen,L.Y., Zhang,Y., Zhang,Q., Li,H., Luo,Z., Fang,H., Kim,S.H., Qin,L., Yotnda,P., Xu,J. *et al.* (2012) Mitochondrial localization of telomeric protein TIN2 links telomere regulation to metabolic control. *Mol. Cell*, **47**, 839–850.
24. Sullivan,L.B., Santos,J.H. and Chandel,N.S. (2012) Mitochondria and telomeres: the promiscuous roles of TIN2. *Mol. Cell*, **47**, 823–824.
25. Chen,L.Y., Liu,D. and Songyang,Z. (2007) Telomere maintenance through spatial control of telomeric proteins. *Mol. Cell. Biol.*, **27**, 5898–5909.
26. Good,P.J. (1995) A conserved family of elav-like genes in vertebrates. *Proc. Natl. Acad. Sci. U.S.A.*, **92**, 4557–4561.
27. Ma,W.J., Cheng,S., Campbell,C., Wright,A. and Furneaux,H. (1996) Cloning and characterization of HuR, a ubiquitously expressed Elav-like protein. *J. Biol. Chem.*, **271**, 8144–8151.
28. Brennan,C.M. and Steitz,J.A. (2001) HuR and mRNA stability. *Cell. Mol. Life Sci.*, **58**, 266–277.
29. Hinman,M.N. and Lou,H. (2008) Diverse molecular functions of Hu proteins. *Cell. Mol. Life Sci.*, **65**, 3168–3181.
30. Kim,H.H. and Gorospe,M. (2008) Phosphorylated HuR shuttles in cycles. *Cell Cycle*, **7**, 3124–3126.
31. Levy,N.S., Chung,S., Furneaux,H. and Levy,A.P. (1998) Hypoxic stabilization of vascular endothelial growth factor mRNA by the RNA-binding protein *HuR*. *J. Biol. Chem.*, **273**, 6417–6423.
32. Wang,W., Furneaux,H., Cheng,H., Caldwell,M.C., Hutter,D., Liu,Y., Holbrook,N. and Gorospe,M. (2000) HuR regulates p21 mRNA stabilization by UV light. *Mol. Cell. Biol.*, **20**, 760–769.
33. Dean,J.L., Wait,R., Mahtani,K.R., Sully,G., Clark,A.R. and Saklatvala,J. (2001) The 3′ untranslated region of tumor necrosis factor alpha mRNA is a target of the mRNA-stabilizing factor HuR. *Mol. Cell. Biol.*, **21**, 721–730.
34. Sengupta,S., Jang,B.C., Wu,M.T., Paik,J.H., Furneaux,H. and Hla,T. (2003) The RNA-binding protein HuR regulates the expression of cyclooxygenase-2. *J. Biol. Chem.*, **278**, 25227–25233.
35. Dormoy-Raclet,V., Ménard,I., Clair,E., Kurban,G., Mazroui,R., Di Marco,S., von Roretz,C., Pause,A. and Gallouzi,I.E. (2007) The RNA-binding protein HuR promotes cell migration and cell invasion by stabilizing the beta-actin mRNA in a U-rich-element-dependent manner. *Mol. Cell. Biol.*, **27**, 5365–5380.
36. López de Silanes,I., Gorospe,M., Taniguchi,H., Abdelmohsen,K., Srikantan,S., Alaminos,M., Berdasco,M., Urdinguio,R.G., Fraga,M.F., Jacinto,F.V. *et al.* (2009) The RNA-binding protein HuR regulates DNA methylation through stabilization of DNMT3b mRNA. *Nucleic Acids Res.*, **37**, 2658–2671.
37. Kim,H.H., Kuwano,Y., Srikantan,S., Lee,E.K., Martindale,J.L. and Gorospe,M. (2009) HuR recruits let-7/RISC to repress c-Myc expression. *Genes Dev.*, **23**, 1743–1748.
38. Chang,N., Yi,J., Guo,G., Liu,X., Shang,Y., Tong,T., Cui,Q., Zhan,M., Gorospe,M. and Wang,W. (2010) HuR uses AUF1 as a cofactor to promote p16INK4 mRNA decay. *Mol. Cell. Biol.*, **30**, 3875–3886.
39. Wang,W., Yang,X., Lopez de Silanes,I., Carling,D. and Gorospe,M. (2003) Increased AMP:ATP ratio and AMP-activated protein kinase activity during cellular senescence linked to reduced HuR function. *J. Biol. Chem.*, **278**, 27016–27023.
40. Wang,W., Yang,X., Cristofalo,V.J., Holbrook,N.J. and Gorospe,M. (2001) Loss of HuR is linked to reduced expression of proliferative genes during replicative senescence. *Mol. Cell. Biol.*, **21**, 5889–5898.
41. Yi,J., Chang,N., Liu,X., Guo,G., Xue,L., Tong,T., Gorospe,M. and Wang,W. (2010) Reduced nuclear export of HuR mRNA by HuR is linked to the loss of HuR in replicative senescence. *Nucleic Acids Res.*, **38**, 1547–1155.
42. Kawagishi,H., Hashimoto,M., Nakamura,H., Tsugawa,T., Watanabe,A., Kontoyiannis,D.L. and Sugimoto,M. (2013) HuR maintains a replicative life span by repressing the ARF tumor suppressor. *Mol. Cell. Biol.*, **33**, 1886–1900.
43. Davalli,P., Mitic,T., Caporali,A., Lauriola,A. and D'Arca,D. (2016) ROS, cell senescence, and novel molecular mechanisms in aging and age-related diseases. *Oxid. Med. Cell. Longev.*, **2016**, 3565127.
44. Passos,J.F., Saretzki,G. and von Zglinicki,T. (2007) DNA damage in telomeres and mitochondria during cellular senescence: is there a connection? *Nucleic Acids Res.*, **35**, 7505–7513.
45. Passos,J.F., Nelson,G., Wang,C., Richter,T., Simillion,C., Proctor,C.J., Miwa,S., Olijslagers,S., Hallinan,J., Wipat,A. *et al.* (2010) Feedback between p21 and reactive oxygen production is necessary for cell senescence. *Mol. Syst. Biol.*, **6**, 347.
46. Bustin,S.A., Benes,V., Garson,J.A., Hellemans,J., Huggett,J., Kubista,M., Mueller,R., Nolan,T., Pfaffl,M.W., Shipley,G.L. *et al.* (2009) The MIQE guidelines: minimum information for publication of quantitative real-time PCR experiments. *Clin. Chem.*, **55**, 611–622.

47. Lee,G.E., Yu,E.Y., Cho,C.H., Lee,J., Muller,M.T. and Chung,I.K. (2004) DNA-protein kinase catalytic subunit interacting protein KIP binds telomerase by interacting with human telomerase reverse transcriptase. *J. Biol. Chem.*, **279**, 34750–34755.
48. Kim,Y., Noren Hooten,N., Dluzen,D.F., Martindale,J.L., Gorospe,M. and Evans,M.K. (2015) Posttranscriptional regulation of the inflammatory marker C-reactive protein by the RNA-binding protein HuR and microRNA 637. *Mol. Cell. Biol.*, **35**, 4212–4221.
49. Abreu,E., Terns,R.M. and Terns,M.P. (2011) Visualization of human telomerase localization by fluorescence microscopy techniques. *Methods Mol. Biol.*, **735**, 125–137.
50. Lee,J.H., Jeong,S.A., Khadka,P., Hong,J. and Chung,I.K. (2015) Involvement of SRSF11 in cell cycle-specific recruitment of telomerase to telomeres at nuclear speckles. *Nucleic Acids Res.*, **43**, 8435–8451.
51. Her,Y.R. and Chung,I.K. (2013) p300-mediated acetylation of TRF2 is required for maintaining functional telomeres. *Nucleic Acids Res.*, **41**, 2267–2283.
52. Abdelmohsen,K., Kuwano,Y., Kim,H.H. and Gorospe,M. (2008) Posttranscriptional gene regulation by RNA-binding proteins during oxidative stress: implications for cellular senescence. *Biol. Chem.*, **389**, 243–255.
53. Itahana,K., Dimri,G. and Campisi,J. (2001) Regulation of cellular senescence by p53. *Eur. J. Biochem.*, **268**, 2784–2791.
54. Brown,J.P., Wei,W. and Sedivy,J.M. (1997) Bypass of senescence after disruption of p21CIP1/WAF1 gene in normal diploid human fibroblasts. *Science*, **277**, 831–834.
55. Serrano,M., Lin,A.W., McCurrach,M.E., Beach,D. and Lowe,S.W. (1997) Oncogenic ras provokes premature cell senescence associated with accumulation of p53 and p16INK4a. *Cell*, **88**, 593–602.
56. Takai,H., Smogorzewska,A. and de Lange,T. (2003) DNA damage foci at dysfunctional telomeres. *Curr. Biol.*, **13**, 1549–1556.
57. Yoo,H.H. and Chung,I.K. (2011) Requirement of DDX39 DEAD box RNA helicase for genome integrity and telomere protection. *Aging Cell*, **10**, 557–571.
58. Hewitt,G., Jurk,D., Marques,F.D., Correia-Melo,C., Hardy,T., Gackowska,A., Anderson,R., Taschuk,M., Mann,J. and Passos,J.F. (2012) Telomeres are favored targets of a persistent DNA damage response in ageing and stress-induced senescence. *Nat. Commun.*, **3**, 708.
59. Cong,Y.S., Wright,W.E. and Shay,J.W. (2002) Human telomerase and its regulation. *Microbiol. Mol. Biol. Rev.*, **66**, 407–425.
60. Srikantan,S. and Gorospe,M. (2012) HuR function in disease. *Front Biosci. (Landmark Ed)*, **17**, 189–205.
61. Wang,J., Guo,Y., Chu,H., Guan,Y., Bi,J. and Wang,B. (2013) Multiple functions of the RNA-binding protein HuR in cancer progression, treatment responses and prognosis. *Int. J. Mol. Sci.*, **14**, 10015–10041.
62. Lu,T. and Finkel,T. (2008) Free radicals and senescence. *Exp. Cell Res.*, **314**, 1918–1922.
63. Kuilman,T., Michaloglou,C., Mooi,W. J. and Peeper,D.S. (2010) The essence of senescence. *Genes Dev.*, **24**, 2463–2479.
64. Zarei,M., Lal,S., Parker,S.J., Nevler,A., Vaziri-Gohar,A., Dukleska,K., Mambelli-Lisboa,N.C., Moffat,C., Blanco,F.F., Chand,S.N. *et al.* (2017) Posttranscriptional upregulation of IDH1 by HuR establishes a powerful survival phenotype in pancreatic cancer cells. *Cancer Res.*, **77**, 4460–4471.
65. Indran,I.R., Hande,M.P. and Pervaiz,S. (2011) hTERT overexpression alleviates intracellular ROS production, improves mitochondrial function, and inhibits ROS-mediated apoptosis in cancer cells. *Cancer Res.*, **71**, 266–276.